NASA TECHNICAL NOTE

NASA TN D-7674

NASA TN D-7674

AERODYNAMIC DRAG AND FUEL SPREADING MEASUREMENTS IN A SIMULATED SCRAMJET COMBUSTION MODULE

by Louis A. Povinelli

Lewis Research Center

Cleveland, Ohio 44135

NATIONAL AERONAUTICS AND SPACE ADMINISTRATION • WASHINGTON, D. C. • MAY 1974

1. Report No.	2. Government Accession No.	3. Recipient's Catalog No.
NASA TN D-7674		

4. Title and Subtitle	5. Report Date
AERODYNAMIC DRAG AND FUEL SPREADING MEASUREMENTS IN A SIMULATED SCRAMJET COMBUSTION MODULE	MAY 1974
	6. Performing Organization Code

7. Author(s)	8. Performing Organization Report No.
Louis A. Povinelli	E-7849
	10. Work Unit No. 501-24

9. Performing Organization Name and Address	11. Contract or Grant No.
Lewis Research Center National Aeronautics and Space Administration Cleveland, Ohio 44135	
	13. Type of Report and Period Covered
12. Sponsoring Agency Name and Address	Technical Note
National Aeronautics and Space Administration Washington, D.C. 20546	14. Sponsoring Agency Code

15. Supplementary Notes

16. Abstract

The drag of a simulated scramjet combustion module was measured at Mach 2, 2.5, and 3. The combustor was rectangular in cross section and incorporated six swept fuel injector struts. The effect of strut leading edge radius, position of maximum thickness, thickness ratio, sweep angle, and strut length on the drag was determined. Reduction in thickness ratio had the largest effect on drag reduction. Sweeping the struts upstream yielded the same drag as sweeping the struts downstream and potentially offers the advantages of increased mixing time for the fuel. Helium injection was used to simulate hydrogen fuel. The interstrut spacing required to achieve good distribution of fuel was found to be about 10 jet diameters. The contribution of helium injection to drag reduction was small.

17. Key Words (Suggested by Author(s))	18. Distribution Statement
Scramjet combustors Fuel penetration Scramjet injector drag Hypersonic propulsion	Unclassified - unlimited Category 12

19. Security Classif. (of this report)	20. Security Classif. (of this page)	21. No. of Pages	22. Price*
Unclassified	Unclassified	37	$3.25

* For sale by the National Technical Information Service, Springfield, Virginia 22151

AERODYNAMIC DRAG AND FUEL SPREADING MEASUREMENTS IN A SIMULATED SCRAMJET COMBUSTION MODULE

by Louis A. Povinelli

Lewis Research Center

SUMMARY

The drag of a simulated scramjet combustion module was measured at Mach numbers of 2, 2.5, and 3. The dynamic pressure was varied from 37.9 to 48.3 kN/m^2 (792 to 1008 psfa) and the Reynolds number per meter varied from 35.1×10^6 to 7.8×10^6 (10.6×10^6 to 2.4×10^6 per ft).

Six swept injector struts were installed in the combustor module. The effect of leading edge radius, position of maximum thickness, thickness ratio, sweep angle, and strut length on the drag was measured. The variation in leading edge radius (0.005 to 0.01 chord length) and the position of maximum thickness (0.5 to 0.7 chord length) did not have any significant effect on drag. Reducing the thickness ratio from 0.16 to 0.075 caused a 65 percent reduction in drag. A change in sweepback angle from 60^o to 36^o caused only a small increase in strut drag. Sweeping the struts forward an amount equal to the sweepback did not change the drag and offers the potential of increased residence time for fuel mixing.

Helium was injected to simulate hydrogen fuel. Measurements of the helium concentration were made at a station 1.72 duct heights downstream of the combustor exit. The vertical spacing between struts was varied by using struts of different thickness ratio. The vertical spacing required for achieving reasonable concentration levels was about 10 jet diameters. Helium injection in the downstream direction (from trailing edge orifices in the strut) was found to have a small effect on the drag reduction. For injection with a stoichiometric fuel-air mixture and a free stream Mach number of 2.5, the total combustor drag was reduced by 6 to 9 percent.

INTRODUCTION

This report is concerned with fuel injector design for scramjet combustors. Scramjet propulsion has been considered for hypersonic flight in the Mach 6 to 12 range. Efforts are currently being directed toward the development of individual scramjet modules which could be mounted on the underside of a vehicle as shown in figure 1 (ref. 1). The concept makes use of the vehicle forebody as a compression surface followed by internal compression. Hydrogen injection and combustion occur within the module, followed by expansion. The afterbody of the vehicle is used as an expansion surface.

Only limited information is available for designing an integrated scramjet module. This investigation was carried out to provide design information for the fuel injectors used in the combustor section. The study is specifically concerned with fuel distribution patterns obtained with various strut configurations and the associated drag measured over a Mach number range of 2 to 3. This range corresponds to typical combustor inlet conditions. Testing was performed in a 0.31- by 0.31-meter (1- by 1-ft) wind tunnel at Reynolds numbers per meter of 35.1×10^6 to 7.8×10^6 (10.6×10^6 to 2.4×10^6 per ft).

APPARATUS AND PROCEDURE

Wind Tunnel

The tests were conducted at Mach 2.0, 2.5, and 3.0 (nominal) in a 0.31- by 0.31-meter (nominal 1- by 1-ft) wind tunnel. Calibration and starting data are given in appendix A. The total temperature of the air stream was 294.4 K (530° R) and the total pressure was varied from 100 to 276 kN/m^2 (14.5 to 40 psia). The corresponding values of dynamic pressure $q = (\gamma/2)p_\infty M_\infty^2$ were 37.9 to 48.3 kN/m^2 (792 to 1008 psfa). Symbols are defined in appendix B. The free stream Reynolds number per meter varied from 35.1×10^6 to 7.8×10^6 (10.6×10^6 to 2.4×10^6 per ft).

Simulated Combustor Module

The simulated combustor section was installed in the test section of the tunnel. The rectangular cross section was 22.85 centimeters (9 in.) high by 30.5 centimeters (12.2 in.) wide. The side plates were 40.8 centimeters (16 in.) long and were flush with the inside wall of the wind tunnel (see fig. 2(a)). The top and bottom walls of the test section were 66 centimeters (26 in.) long and had a 15° wedge angle on the leading and trailing edges. The wall thickness was 0.64 centimeter (0.25 in.). The combustor was mounted on six linear motion bearings which allowed it to move in the longitudinal

direction of the tunnel. The motion was restrained by a load cell (444.8 N or 100 lbf) as shown in figure 2(b). The housings which contained the linear bearings were mounted to a pressure box which in turn was fixed to the external tunnel wall. In this fashion, the load created by the combustor section and the strut could be measured. Figure 2(c) shows an exterior view of the combustor side wall, with the cover plate removed from the pressure box. Figure 2(c) also shows the three ports for strut installations. The upstream port was located on the tunnel centerline and the two ports downstream were 7.63 centimeters (3 in.) apart, and 3.82 centimeters (1.5 in.) from the centerline. The longitudinal spacing between the two port stations was 30.5 centimeters (12 in.). The opposite side of the tunnel was arranged the same way.

Clearance between the combustor section and the tunnel walls was maintained at 0.051 centimeter (0.020 in.), as shown in figure 2(b). This clearance was also maintained between the extended portions of the top and bottom plates and the side wall of the tunnel (refer to fig. 2(b)). The external pressure box eliminated the need for complicated seals between the moveable section and the tunnel walls.

The drag balance was calibrated by weights suspended from a pulley arrangement. Periodic calibration of the drag system was made throughout the testing program. The accuracy of the drag balance was ±2.2 newtons (±0.5 lbf) over the load range.

Static pressure taps were installed along the centerline of the top and bottom plates of the combustor, as shown in figure 2(d). Pressure taps were also placed on the bottom plate halfway between the tunnel side wall and the tunnel centerline. Bulkhead fittings were used to lead the pressure connections through the pressure box to pressure transducers.

Strut Geometries

Nine different strut geometries were selected for testing. The baseline or reference design was essentially that used by Metzler and Mertz (ref. 2) in supersonic combustor testing (fig. 3). All of the struts were symmetrical double wedges and had sweepback. Each strut had 18 orifices located as shown in figure 3. Six of the orifices were located on the ridgeline on both sides of the struts. The remaining six orifices were located on the trailing edge of the strut. (Injection from the trailing edge was expected to yield a small amount of thrust thereby reducing the overall drag.) For some of the tests, an additional orifice was drilled in the tip of the strut as shown in figure 3. The location of the orifices duplicates that of reference 2 which was used in a cylindrical combustor. The modifications to the baseline design (strut 1) are shown in the table of figure 3. Strut 2 duplicates the basic strut but has a leading edge radius which is only one-half as large. The trailing edge radii were the same for all struts ($r/l_1 = 0.005$). Strut 3 has its maximum thickness at the 50 percent chord point. Struts 4 and 5 are reduced in

thickness ($\delta = t/l_1$) to 10 and 7.5 percent, respectively. Struts 6, 7, and 8 have less sweepback Λ_1, and strut 9 is the same as strut 4 except it was reduced in length from 12.7 to 10.4 centimeters (5 to 4.1 in.). The thickness ratio was constant along the strut (root to top) for all the geometries. The struts were fabricated as a shell from 16 gauge stainless steel (0.151 cm or 0.0595 in.). Four internal pins were welded into place inside the shell to provide support. This construction resulted in some surface waviness of the struts.

Fuel Injection and Distribution Measurements

Helium was used to simulate the injection of hydrogen. The amount of helium injected was varied in accordance with the mass flow of the airstream in order to obtain a stoichiometric fuel-air mixture. The combustor section had a frontal area of 22.9 by 30.5 centimeters (9 by 12 in.) which amounts to 75 percent of the test section area. It was assumed that three-fourths of the air passed through the combustor. The helium flow rate was determined from measurements across an orifice plate. The injection pressure of the helium was adjusted so that the helium mass flow for the final strut configuration was 3 percent of the airflow. Prior to tunnel operation, internal strut pressure was measured. The flow through the injection orifices was found to be choked.

Samples were withdrawn from the flow stream using a wedge rake with 15 pitot probe tips. Each tip was made of 0.076 centimeter (0.030 in.) O.D. stainless tube with 0.0076 centimeter (0.003 in.) wall and protruded forward from the wedge a distance of 0.152 centimeter (0.06 in.). The center-to-center spacing of the probe tips was 0.508 centimeter (0.2 in.). The probe tips were connected to a 12 position scanning valve (rendering three randomly spaced tips inoperative). The probe is shown in figure 2(a), upstream of the combustor section. When taking gas samples, the probe was installed downstream of the combustor section and located on the tunnel side wall. The sampling rake was located at 1.72 duct (combustor) heights ($x/h = 4.50$) downstream of the trailing edge of the top and bottom plates. The probe was mounted on an actuator mechanism on the side wall of the tunnel. Two mounting positions on the side wall were used; one on the tunnel centerline, the other was located 6.99 centimeters (2.75 in.) above the tunnel centerline. With these two positions it was possible to determine the presence of helium in approximately one-half of the combustor.

The samples were continuously analyzed by a mass spectrometer for the amount of helium present in the sample. Sampling pressure was manually regulated to maintain a value of 20 mm Hg abs. The sampling system is described in reference 3.

A helium manifold was installed inside the pressure box. Flexible tubing was used to connect the manifold to the struts. Calibration checks were made on the drag system to ensure that the manifold did not create a load on the combustor section.

RESULTS AND DISCUSSION

Pressure Distribution

The origin of the coordinate system and the static pressure distribution measured along the combustor section (in the absence of struts) are shown in figure 4(a). The measurements were made at the three values of the dynamic pressure shown in the figure. The upstream data are seen to scatter around the pressure ratio corresponding to Mach 2.5. A slight pressure rise is noted downstream ($x/h \approx 2$) at the top wall. The increase in pressure may have been partly caused by some waviness in the bottom plate of the combustor. Part of the pressure rise may also be due to the effect of skin friction. Figure 4(a) shows the theoretical increase in pressure due to friction assuming an average friction coefficient of 0.0036. (The pressure rise due to friction was calculated assuming one-dimensional adiabatic flow.) This value of the coefficient was based on the drag measurements presented in the next section. The variation in static pressure was 0.69 to 1.38 kN/m^2 (0.1 to 0.2 psi) and the accuracy of the pressure measurements was 0.69 kN/m^2 (0.1 psi). The observed difference between the calculated and measured rise in pressure may be attributable to the inaccuracies of the pressure measurements.

The static pressure distribution, measured with two struts located at the upstream station (one strut on each side of the combustor) is shown in figure 4(b). The shock waves due to the presence of the struts caused a two-fold rise in static pressure at the rearward section of the combustor, both at the top and bottom walls. For reference purposes the data with no struts are also shown in the figure. The pressure distribution was also measured with six struts installed in the combustor (as shown in fig. 2(a)). The resulting distribution was identical to that shown in figure 4(b). The shock waves caused by the four (downstream) struts, evidently, intersected the tunnel wall downstream of the combustor section. Hence the measured pressure distribution along the combustor section walls was affected by the upstream struts only.

The pressure distribution was also measured while helium was injected through the strut injectors. Peak pressures were observed to be slightly higher with helium injection.

Skin Friction Drag

The measured drag of the combustor with no struts is shown in figure 5. This drag is due to the effect of skin friction and to the plate thickness (0.64 cm or 0.25 in.). Both the top and bottom plates of the combustor are immersed in the flow stream and contribute to thickness drag. The thickness (pressure) drag may be calculated using the fol-

lowing expression for the drag coefficient:

$$C_{D,th} = \frac{2\Delta^2}{\sqrt{M_\infty^2 - 1}}$$

where $\Delta = (T/L_1)_{plate}$. Substituting yields

$$C_{D,th} = 8.73 \times 10^{-5}$$

The thickness drag may be calculated from

$$D_{th} = \frac{\gamma}{2} p_\infty M_\infty^2 C_{D,th} L_1 w$$

where L_1 is the length of the top or bottom wall of the combustor (66.1 cm or 26 in.) and w is the width (31 cm or 12.2 in.). The resulting values for thickness drag are as follows:

Dynamic pressure, q		Drag, D	
kN/m^2	psfa	N	lbf
37.9	792	1.33	0.30
43.4	907	1.53	.34
48.3	1008	1.70	.38

The calculated thickness drag values are seen to be very small and may be neglected. The drag data shown in figure 5, therefore, may be considered to be due to the effect of skin friction alone. In order to evaluate an average skin friction coefficient, we write

$$\overline{C_f} = \frac{D_f}{q(4L_1 w + 2hL_2)}$$

where the wetted area is $4L_1 w + 2hL_2$. Evaluating the previous equation at the three q values yields the average friction coefficient

$$\overline{C}_f = 0.0036$$

Using this value of $\overline{C}_f$ to calculate drag gives the line shown in figure 5.

Strut Drag

Reference strut drag. - The drag of the combustor module with six struts (number 1 shown in fig. 3) was measured at Mach 2.5 at three dynamic pressure conditions. The result is shown in figure 6. The addition of six struts increased the drag 190 newtons (43 lbf) at the lowest pressure condition. The drag per strut amounts to about 32 newtons (7 lbf). At the highest dynamic pressure, 48.3 kN/m^2 (1008 psfa), the drag increased 245 newtons (55 lbf) which is approximately 41 newtons (9 lbf) per strut. Drag measurements were also made with only two struts installed in the module. The drag caused by the two struts mounted upstream was 66.7, 73.4, and 80 newtons (15, 16.5, and 18 lbf) at the three dynamic stream conditions. The drag per strut again amounted to approximately 33, 37, and 40 newtons (7, 8, and 9 lbf). The strut drag appears, therefore, to be linearly dependent on the number of struts.

Drag measurements were also made with only two struts installed at the rearward station. The results are shown in figure 6. The drag values are very close for both cases. Installation of the struts at the forward station caused shock wave intersection at the module wall (as seen in previous static pressure distribution in fig. 4(b)). The rearward installation caused the shock waves to fall outside (downstream) of the combustor section. The fact that the drag was the same with either forward or rearward mounting indicates that the shock wave - boundary layer interactions did not significantly alter the skin friction drag.

Effect of leading edge radius and maximum thickness position . - The effect of leading edge radius on drag was determined by comparison of strut 1 with strut 2. The radius-to-root chord ratio was 0.005 compared to 0.010 for strut 1. Figure 7 shows that the change in radius did not significantly (~1 percent) affect the measured drag. The effect of changing the position of maximum strut thickness also did not cause any noticeable alteration in the drag measurements. Strut 3 had its maximum thickness at the 50 percent chord position compared to 70 percent for strut 2. Measured drag values were the same. Within the range of the variables tested, therefore, the position of maximum thickness and the leading edge radius did not influence the drag force.

Thickness ratio. - Struts 3, 4, and 5 were tested to determine the effect of thickness ratio on drag. The strut drag is shown in figure 8 for the three struts. The con-

tribution of the empty combustor section has been subtracted from the total drag values measured. Reducing the thickness ratio from 0.16 to 0.10 resulted in approximately a 50 percent drag reduction over the entire dynamic pressure range. A further reduction in thickness ratio (from 0.16 to 0.075) resulted in a 60 to 65 percent reduction over the same q range. These results show that the drag per strut ($q = 43.4\ kN/m^2$ or 90 psfa) for the 0.10 thickness geometry is about 17.8 newtons (4 lbf). This value compares with 35.6 newtons (8 lbf) for the 0.16 thickness strut. Therefore, it is possible to reduce combustor drag with the use of the thinner struts. For example, using eight to ten of the 0.10 thickness ratio struts (depending on spacing requirements for proper fuel distribution) gives a drag of 142.4 to 178 newtons (32 to 40 lbf). With six struts, having a 0.16 thickness ratio, the drag is 213.6 newtons (48 lbf). These numbers represent a drag reduction of 17 to 33 percent.

To explain the trend of the data, calculations are made using linear theory. In accordance with linear wing theory, the drag coefficient at zero lift for a double wedge symmetrical airfoil is

$$C_D = \frac{4 \cos^3 \Lambda \, \delta_e^2}{\sqrt{M_\infty^2 \cos^2 \Lambda - 1}},$$

where δ_e is the thickness drag normal to the leading edge and the drag is

$$D_{th} = \frac{4 q_\infty \cos \Lambda \, \delta^2}{\sqrt{M_\infty^2 \cos^2 \Lambda - 1}} \, lS$$

Referring to the preceding equation, it may be seen that, for fixed values of the dynamic pressure q_∞, sweepback Λ, chord length l, strut span S, and Mach number M_∞, the drag is proportional to the thickness ratio squared. Figure 9 is a plot of the experimental strut drag as a function of thickness ratio squared with free stream dynamic pressure as a parameter. At the higher dynamic pressure values the drag is nearly linear with δ^2 whereas at the lower dynamic pressure some deviation is observed. The calculated drag, based on linear wing theory, is in reasonable agreement for the strut with low thickness ratio (δ of 0.075) but is a factor of 2 to 3 higher for the 10 and 16 percent struts. The lack of agreement may be due to the fact that linear theory becomes invalid for large perturbations. Also the finite span of the wing and the effect of strut taper may affect the calculations. Struts 3, 4, and 5 in this study have thick-

ness ratios δ_e of 15, 20, and 32 percent.

Sweep of leading edge. - Reduced sweepback is desirable in order to increase the residence time for the fuel. (Reducing sweepback may be undesirable with respect to thermal choking and leading edge cooling. Neither of these effects are considered in this report.) The effect of reducing sweepback on drag was measured using struts 6, 7, and 8. An attempt was made to optimize the strut design using the theoretical results of Puckett (ref. 4). The three struts were designed with a constant value of sweepback angle to Mach angle ($\Lambda/\beta = 0.6$). The 36°, 40°, and 43° struts were designed for testing at Mach 2, 2.5, and 3, respectively. Testing was extended, however, for a given strut to all three Mach numbers. Typical results are shown in figure 10 for a sweep angle of 40°. It was found that, with all of the struts tested at the three Mach numbers and the range of dynamic pressures, only a small drag increase occurred. Comparison of the strut drag data in figure 10 with those for the 60° sweepback in figure 8 ($\delta = 0.1$) shows a maximum increase in strut drag of 26.7 newtons (6 lbf). Note that figure 8 is a plot of strut drag only, whereas figure 10 is a plot of strut and combustor drag. Over the range of conditions investigated, the increased drag varied from only 1.8 to 4.45 newtons (0.40 to 1 lbf) per strut. The increase in drag, of approximately 25 percent for a 20° change in sweep angle, is in agreement with the data of Vincenti (ref. 5).

Reversed sweep. - Vincenti (ref. 5) has also shown that the minimum pressure (thickness) drag of a swept wing is nearly unchanged by a reversal of the sweep. If this were the case for internal flows it would mean a further increase in fuel residence time within the combustor. (It is noted that reverse sweep may adversely affect inlet performance if the struts protrude upstream of the combustor entrance. The acute angle at the wall may also cause localized boundary layer separation and severe local heating rates. These effects remain to be studied.) Therefore, strut array 5 was reversed so that the injectors pointed upstream. Since the trailing edge angle Λ_2 was 40°, reversing the struts yielded a sweep angle of -50°. The difference in sweepforward and sweepback was 10° (i.e., -50 versus +60). The experimental data of Vincenti shows that changing the sweep angle from 60° to -50° will result in a 25 percent increase in the drag coefficient (ref. 5). The results of this study are shown in figure 11. The sweptforward struts yielded 12, 18, and 24 percent greater drag than the sweptback struts at dynamic pressures of 37.9, 43.4, and 48.3 kN/m^2 (792, 907, and 1008 psfa), respectively. These results are in agreement with the expected increase in the drag coefficient based on reference 5. It is concluded that struts with 60° forward sweep would yield virtually the same drag as 60° sweepback and would contribute substantially to the residence time of the fuel in the combustor. (It should also be noted that the trailing edge orifices were soldered closed when the blades were swept upstream. The orifices were closed so as not to cause strong local disturbances along the edge of the strut.)

Strut length. - The sum of the thickness drag and skin friction drag is given by the expression

$$D = 2\ell S q_\infty \left(\frac{2 \cos \Lambda \, \delta^2}{\sqrt{M_\infty^2 \cos^2 \Lambda - 1}} + \overline{C}_f \right)$$

For constant values of the dynamic pressure q_∞, sweepback Λ, thickness ratio δ, Mach number M_∞, and friction coefficient $\overline{C}_f$, the drag is proportional to the planform area of the struts. The span of strut 9 was 10.4 centimeters (4.1 in.) compared to 12.7 centimeters (5 in.) for strut 4. The reduction in planform area between the two struts is 12.9 percent. The drag of struts 9 were measured at Mach 2.5 and found to be lower than struts 4. The reduction in drag at a dynamic pressure value of 48.3 kN/m^2 (1008 psfa) was 7 percent and at 43.4 kN/m^2 (907 psfa), the reduction was 8 percent. The magnitude of the strut drag being measured was about 111 newtons (25 lbf). The accuracy of the drag balance was ±2.23 newtons (±0.5 lbf) which amounts to 4 percent of the measurement. Hence, the difference between the calculated decrease (12.9 percent) and the measured decrease may be attributable to the inaccuracy of the drag system and/or finite span or strut taper effects. It was concluded that the decreased drag is proportional to the change in strut length.

Distribution of Injectant

Sampling measurements showed that helium injected from the struts on one side of the combustor did not reach the (lateral) tunnel centerline. It was therefore assumed that lateral symmetry existed in the test section and sampling was carried out over half the tunnel width. Injection was made through three struts only. This procedure also reduced the quantity of helium required for testing.

Three different strut geometries were used in the sampling tests, namely, struts 2, 5, and 8. The center-to-center strut spacing (s in fig. 12(a)) was fixed at 3.81 centimeters (1.5 in.). The minimum vertical distance (c in fig. 12(a)) between the strut surfaces varied with the thickness ratio of the struts. The minimum vertical distance between the strut surfaces occurred at the ridge line of the struts and (due to strut taper) varied from the strut root to the strut tip. The vertical distances are given in the following table:

Strut	Vertical strut spacing (c in fig. 12)			
	Root		Tip	
	cm	in.	cm	in.
2	1.27	0.50	2.44	0.96
5	2.24	.88	2.95	1.16
8	2.64	1.04	3.15	1.24

Figure 12(b) shows the concentration results obtained with struts 8 in a Mach 3.0 airstream. The particular results shown are for a fixed lateral position in the stream ($z/h = 0.222$) and a fixed downstream position of 1.72 combustor heights ($x/h = 4.50$). The mass flow ratio of helium to air was 0.021. The relative strut positions are also shown in the figure. It is seen from these results that the concentration between the struts falls to nearly zero, indicating that very little helium has spread out and filled that region. The diameter of the orifices was 0.36 centimeter (0.141 in.). The injection pressure of the helium was increased to obtain greater penetration. However, the void regions still remained. The higher injection pressure corresponded to helium to air ratios of 0.07. Results at other lateral positions showed the same qualitative behavior.

Results with strut 5 are shown in figure 13 for various lateral stream positions. The helium to air ratio was 0.032 and the injection differed from the previous case in one manner. That is, the six trailing edge orifices were plugged so that all the helium was injected along the ridge line. With this arrangement the orifices were barely choked. The result is not significantly different from that obtained previously. An obvious void region still exists between adjacent struts. Increasing the injection pressure did not alter the results nor did a lowering of free stream Mach number (2.5). Use of smaller diameter orifices to ensure choked flow (0.132 cm or 0.052 in. diam.) also did not change the observed behavior.

The results with struts 2 are shown in figure 14 for two helium to air ratios. It may be seen that relative concentration between the struts is approximately 45 percent. The reduction in strut spacing (dimension c), in going from strut 8 to 2, has been sufficient to yield desirable spreading in the distance available. Increasing the helium to air ratio does not appreciably alter the qualitative behavior. These tests were also run with struts having no trailing edge orifices. This particular strut array was probed in some detail and is shown in figure 15 for various lateral stream positions. It may be seen that the helium distribution depends strongly on the lateral position. Also, sampling directly downstream of an orifice will yield high helium concentrations in the region between the

struts. The orifice spacing along the strut may be somewhat larger (10.8 to 17.7 jet diameters) than needed.

The final strut modification was to redrill the trailing edge orifices halfway between the ridge orifices and to drill one injection hole on the strut tip (see fig. 3 for tip hole location). All of the orifices were 0.132 centimeter (0.052 in.) in diameter. Detailed sampling was carried out; measurements were made at 0.635-centimeter (0.25-in.) intervals in the lateral direction z and at 0.508-centimeter (0.20-in.) intervals in the vertical direction y and contours of the concentration were plotted in figure 16. The downstream location was constant (x/h = 4.50). Superimposed on the concentration contours are the projections of the two downstream struts and the upstream strut. In general, low concentrations of helium ($\leq$50 percent) were found downstream of the middle strut. The higher concentration region ($\leq$95 percent) appeared downstream of the upper and lower struts. Since the helium injected upstream had a longer residence time in the combustor, more mixing occurred, leading to lower concentration levels at the sampling station. Several small regions of high concentration are seen between the upper and middle struts and may be associated with nonuniform flow turning. In general, the helium was distributed over the entire flow area. Further strut refinements such as a reduction in the orifice spacing (e.g., 6 to 10 jet diameters) may improve the distribution.

The concentration contours shown in figure 16 were computer generated using a FORTRAN subroutine for contour plotting. This subroutine was used in conjunction with a bivariate interpolation method and smooth surface fitting based on local procedures. The programming was carried out by Mr. John Riehl of the Lewis Research Center.

Influence of Helium Injection on Drag Measurements

Drag measurements with the final strut modification (described in previous section) were made both with and without helium injection. Injection was made through only three struts, using the amount of helium required for a stoichiometric mixture. At a dynamic pressure of about 37.9 kN/m^2 (790 psfa), the decrease in drag with injection was 8.9 newtons (2 lbf) or approximately 3 newtons (0.66 lbf) per strut. This drag reduction represents about 6 percent of the total drag as shown in figure 7. For struts with low thickness ratios (t/ℓ_1 = 0.075 to 0.10), the measured reduction would be 8 to 9 percent (based on the drag values shown in fig. 8).

No drag decrease due to injection was noted for those struts tested without trailing edge injection. In fact, injection through the ridge orifices only, showed an increase in overall drag which was comparable to the accuracy of the drag balance (±2.2 N or ±0.5 lbf).

CONCLUSIONS

The drag of a rectangular scramjet combustion module having six swept injector struts was measured at Mach 2, 2.5, and 3. The dynamic pressure was varied from 37.9 to 48.3 kN/m^2 (792 to 1008 psfa) and the free stream Reynolds number per meter varied from 35.1×10^6 to 7.8×10^6 (10.6×10^6 to 2.4×10^6 per ft). The contribution of the combustor, without struts, to the drag (i.e. skin friction drag) was also measured. At Mach 2.5 the average friction coefficient was 0.0036.

The effect of the following variables on strut drag were investigated:

(1) Leading edge radius

(2) Position of maximum thickness

(3) Thickness ratio

(4) Sweep angle

(5) Strut length

Among these variables, thickness ratio was found to be the most significant. Reducing thickness ratio form 0.16 to 0.10 caused a 50 percent decrease in drag over the entire dynamic pressure range. The major significance of these results is that the use of a larger number of thin struts rather than thick struts should result in lower overall drag. The greater number of thinner struts would also be helpful in obtaining uniform fuel distribution. The leading edge radius change (r/l_1 from 0.005 to 0.01) and the position of maximum thickness (b from 0.5 to 0.7) did not significantly affect the drag measurements. A decrease in sweepback angle (Λ_1 of 60, 43, 40, and 36) caused a small increase in strut drag. This result is of interest since reduced sweepback offers the potential of more time for fuel mixing within the combustor. A complete reversal of the sweep, that is, sweepforward rather than sweepback, did not significantly affect the drag measurements. Since forward sweep greatly increases combustor residence time, better overall fuel-air mixing could take place with this strut arrangement.

Measurements of the helium concentration were made at a fixed downstream station of 1.72 combustor heights for a fixed strut center-to-center spacing. The results showed that the spacing between strut surfaces had to be of the order of 10 jet diameters apart in order to obtain a reasonable concentration level between struts.

Helium injection at a mass equivalence ratio of unity and a free stream Mach number of 2.5 was found to reduce the total combustor drag by 6 to 9 percent.

Lewis Research Center,
National Aeronautics and Space Adminstration,
Cleveland, Ohio, February 26, 1974,
501-24.

APPENDIX A

WIND TUNNEL CALIBRATION AND BLOCKAGE TESTS

Introduction

The wind tunnel described in this report was reactivated following 12 years of non-use. No calibration data were available regarding the Mach number distribution for the six nozzle blocks. Likewise, no data were available regarding starting blockage. Calibration tests were, therefore, carried out prior to conducting the test program. In order to provide these calibration data for future use, the information obtained is presented herein.

The tunnel is operated on a continuous basis using 862 or 276 kN/m^2 (125 or 40 psig) air supplied by compressors. The air is dried so that condensation-free operation is possible up to Mach 4.0. Exhausters provide 68.5 centimeters (27 in.) Hg vacuum backpressure. A unique feature of this facility is the arrangement for changing Mach number. Figure 17 shows the manner by which the nozzle blocks are changed. The contoured side walls are lifted into place from a carriage, using the flat bottom wall as the lifting platform. Schlieren windows are installed in the top and bottom walls. The frame supporting the Schlieren optics is seen in the background (fig. 17). The frame is moved back to allow for a change in the nozzle blocks.

Nozzle Calibration

Pitot pressures were measured using a five-point rake. The rake installation in the tunnel is shown in figure 17. The spacing on the rake tubes is shown in figure 18. The pitot rake was traversed across the stream so that calibration data were obtained in three horizontal lines or planes (each 5.39 cm or 2.12 in. apart). Static pressures were measured on the top and bottom wall of the test section. The Mach number was calculated from the pressure measurements, assuming constant static pressure across the test section. The Mach number variation for the nozzles in the three lines or planes is shown in figure 19. The corresponding range of static to total pressure ratios was plotted against nominal Mach number in figure 20. The midpoint of the range of $p_1/P_{0,2}$ yields a median Mach number value. These values are equivalent to the average values in figure 19. A schlieren photograph of the calibration rake is shown in figure 21. The angle of the shock wave from the probe tips were measured at a point downstream of the curved shock. For the flow condition shown (Mach 2.5) the measured angle was 24°. The corresponding one-dimensional isentropic Mach number is 2.46. This measurement

was only made as a check on the values determined from the pressure measurements.

Blockage Tests

Blockage tests were conducted using 45° cones mounted in the test section. Tunnel starting was determined from test section static pressure and from schlieren observations. Figure 22 shows the starting sequence for a cone at Mach 2.0. The blockage was approximately 8.5 percent. In figure 22(a), the starting shock is positioned at the cone apex. The Mach reflection (lambda structure) at both walls is evident as well as the formation of slip lines at the shock intersection. As the plenum pressure is increased, the starting shock moves over the cone tip (fig. 22(b)). An oblique shock wave is attached to the cone, followed by the strong normal shock. The vortex lines are now more obvious. Boundary layer separation can be observed on the upper wall. In figure 22(c), the tunnel has started. The oblique (conical) shock is attached to the cone apex and the test section static pressure corresponds to Mach 2.0 flow.

Figure 23 shows the sequence of events for a cone which is too large (blockage of 12 percent) to allow tunnel starting. Figure 23(a) shows the starting shock standing across the tunnel upstream of the cone. Increasing the tunnel total pressure moves the shock over the cone apex (fig. 23(b)). The apex appears to be started. Further increasing the plenum pressure (fig. 23(c)) did not allow the tunnel to start. High turbulence levels and multiple shocks are evident as the cone experiences transonic flow.

The percent blockage created by the various (6) size cones is plotted in figure 24 as a function of Mach number. The starting curve was faired in, based on the individual start and unstart data points.

It is seen that the allowable blockage at Mach 2.5 is approximately 12 percent. This curve was obtained using the 276-kN/m^2 (40-psig) air supply. Some data were obtained with the 862-kN/m^2 (125-psig) air supply. No significant difference in starting behavior was observed.

APPENDIX B

SYMBOLS

b	chord fraction
C	concentration of helium
C_D	drag coefficient
C_f	friction coefficient
c	vertical spacing (see fig. 12)
D	drag
h	combustor height
L_1	combustor length (top and bottom plates)
L_2	combustor length (side plates)
l	chord length
M	Mach number
P_0	total pressure
p	static pressure
q	dynamic pressure, $(\gamma/2)p_\infty M_\infty^2$
r	leading edge radius
S	strut span
s	strut spacing (center to center)
T	combustor thickness (top and bottom plates)
t	strut thickness
w	combustor width
x	downstream (axial) direction
y	vertical direction
z	lateral direction
β	Mach angle
γ	specific heat ratio

Δ thickness ratio, T/L_1

δ thickness ratio, t/l

Λ sweep angle

Subscripts:

e plane normal to leading edge

ef effective

f friction

m mean

max maximum

th thickness

1 strut root or leading edge or upstream

2 strut tip or trailing edge or downstream

∞ free stream

Superscript:

$\overline{}$ average

REFERENCES

1. Henry, J. R.; and Anderson, G. Y.: Design Considerations for the Airframe-Integrated Scramjet. (Presented at the First International Symposium on Air-breathing Engines, Marseille, France, June 19-23, 1972.

2. Metzler, A. J.; and Mertz, T. W.: Preliminary Results of Large Supersonic Burning Combustor Testing. Jour. of Aircraft, vol. 9, no. 1, January 1972, pp. 23-30.

3. Povinelli, Louis A.; Povinelli, Frederick P.; and Hersch, Martin: A Study of Helium Penetration and Spreading in a Mach 2 Airstream Using a Delta Wing Injector. NASA TN D-5322, 1969.

4. Puckett, Allen E.: Supersonic Wave Drag of Thin Airfoils. Jour. Aero. Sciences, vol. 13, no. 9, Sept. 1946, pp. 475-484.

5. Vincenti, Walter G.: Comparison Between Theroy and Experiment for Wings at Supersonic Speeds. NACA TN 2100, 1950.

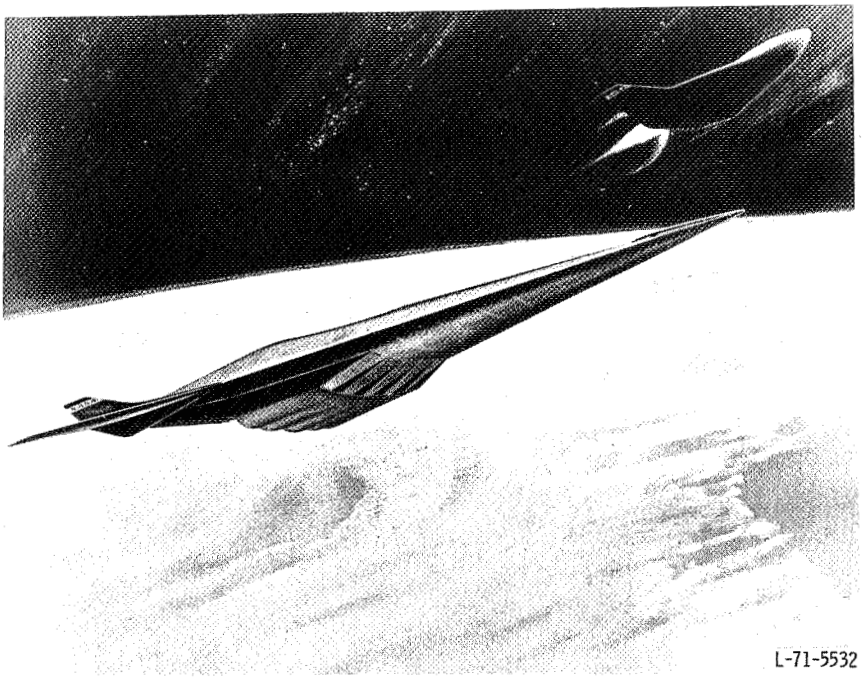

Figure 1. - Hypersonic airbreathing launch vehicle.

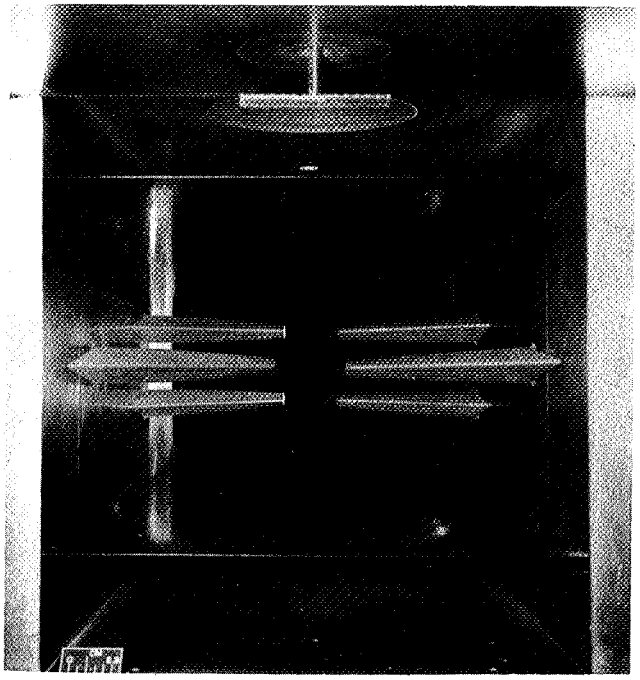

(a) Tunnel installation with number 1 struts. (Downstream view)

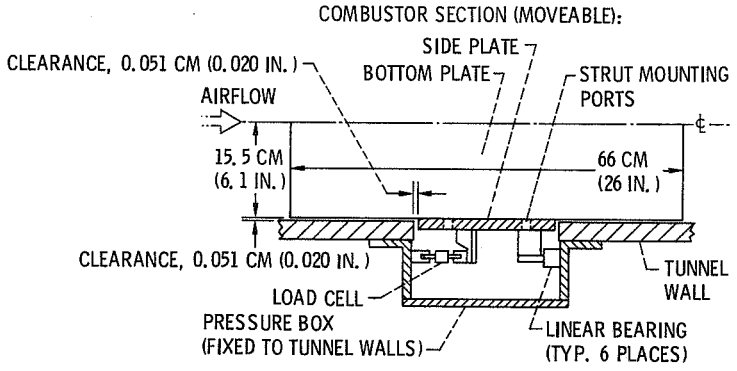

(b) Plan view of combustor installation in wind tunnel.

Figure 2. - Simulated combustor module.

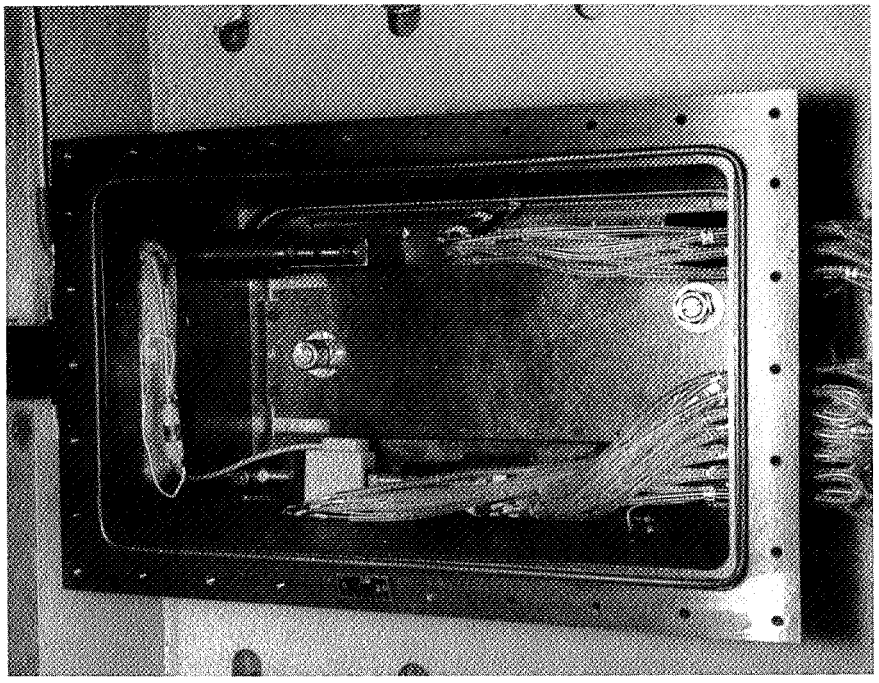

(c) External view of combustor installation (flow left to right).

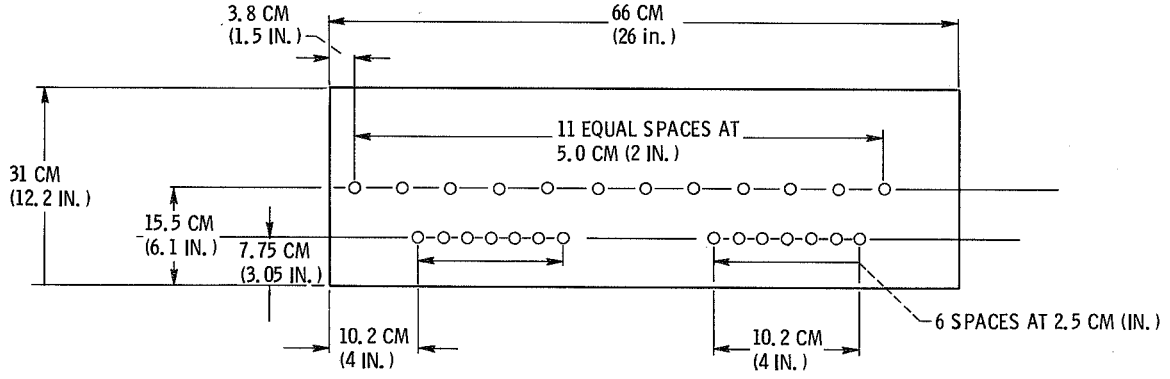

(d) Static pressure tap locations (top and bottom plates).

Figure 2. - Concluded.

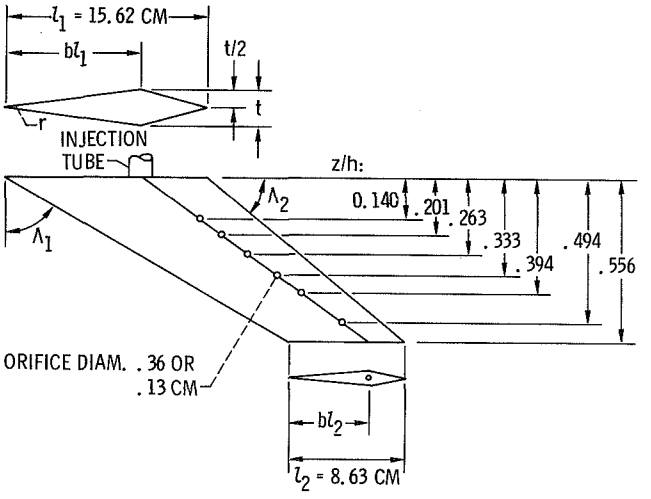

STRUT	r/l_1	Λ_1, deg	Λ_2, deg	b	t/l
1	0.010	60^0	40^0	0.7	0.16
2	.005	60	40	.7	.16
3	.005	60	40	.5	.16
4	.005	60	40	.5	.10
5	.005	60	40	.5	.075
6	.005	36	80	.5	.10
7	.005	40	74	.5	.10
8	.005	43	69	.5	.10
[a]9	.005	60	40	.5	.10

[a]STRUT LENGTH REDUCED TO 10.4 CM FROM 12.7 CM.

Figure 3. - Injection strut geometries.

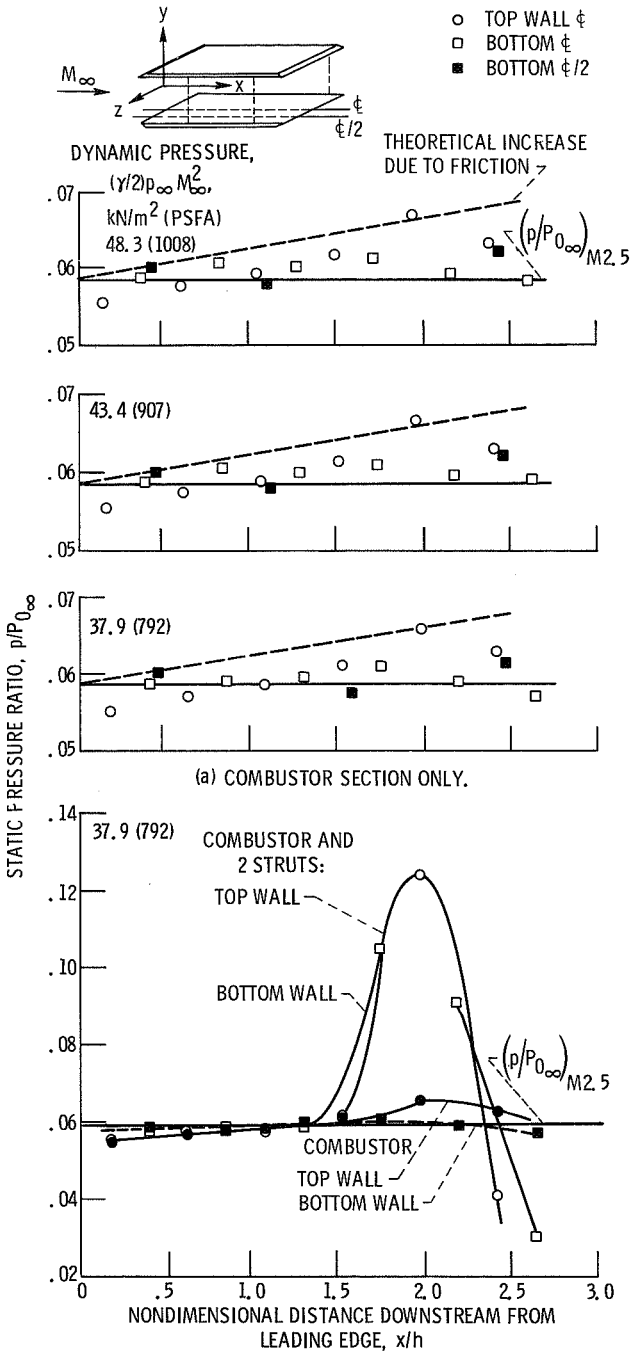

(b) COMBUSTOR AND STRUTS (2 NUMBER 1 STRUTS).

Figure 4. - Static pressure distribution at Mach 2.5.

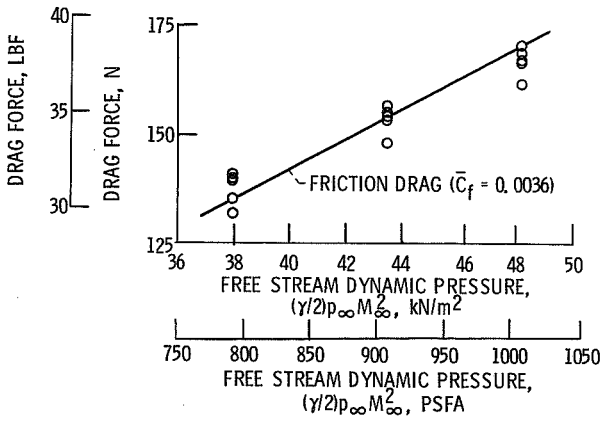

Figure 5. - Combustor section drag measurement (no struts) at Mach 2.5.

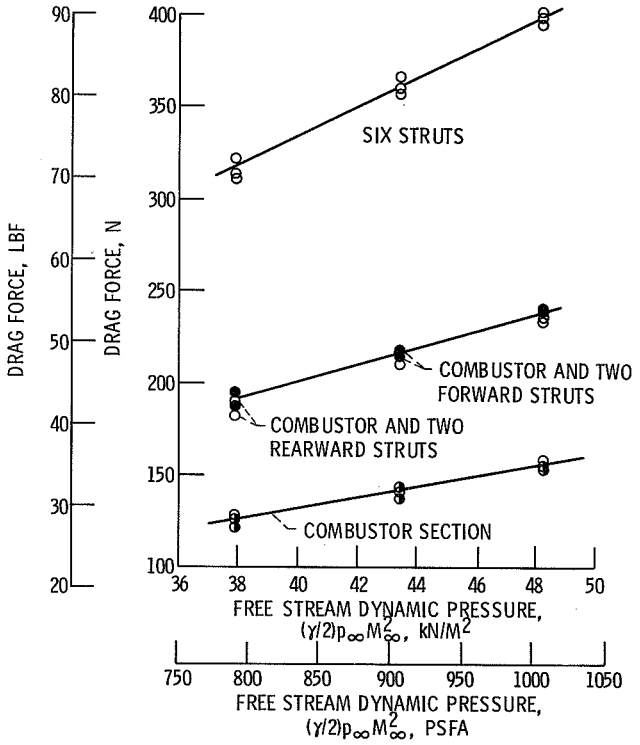

Figure 6. - Drag of combustor module with number 1 struts at Mach 2.5.

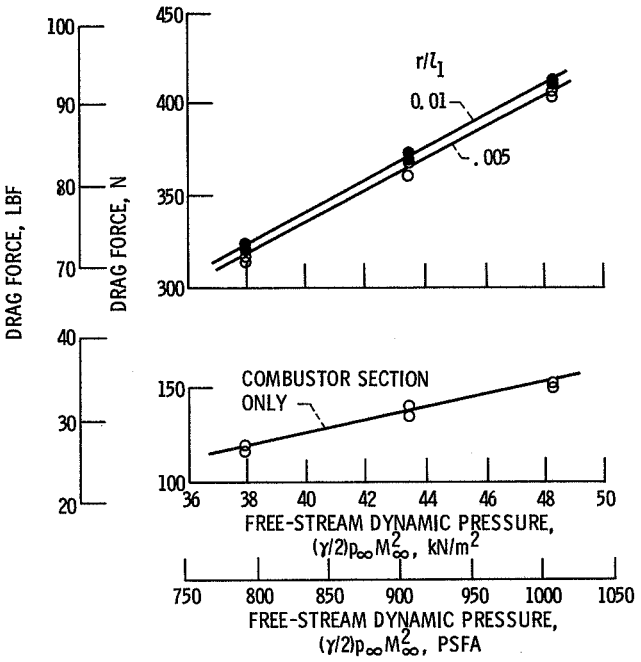

Figure 7. - Effect of leading edge radius on drag at Mach 2.5 with six-strut array.

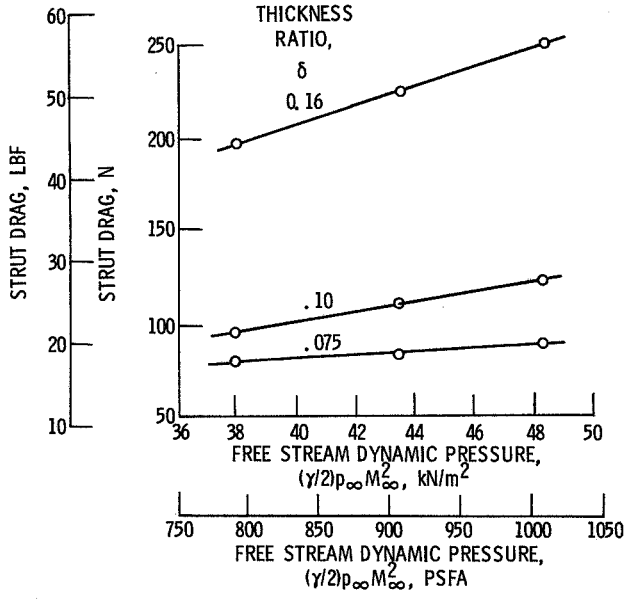

Figure 8. - Effect of strut thickness on drag at Mach 2.5 with six-strut array.

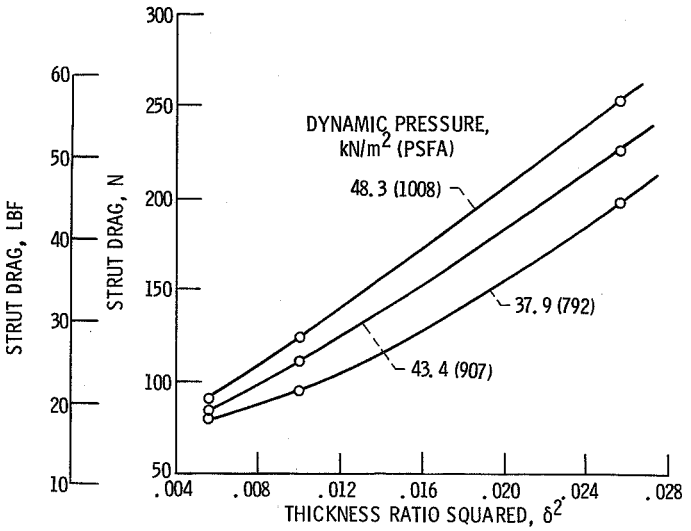

Figure 9. - Experimental strut drag plotted against thickness ratio squared at Mach 2.5.

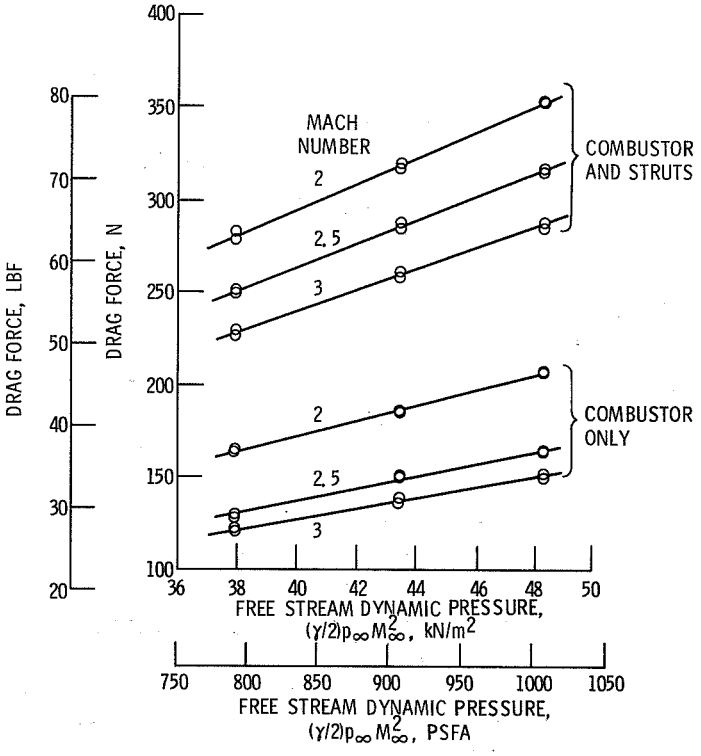

Figure 10. - Experimental drag of strut array (number 7) at various Mach numbers.

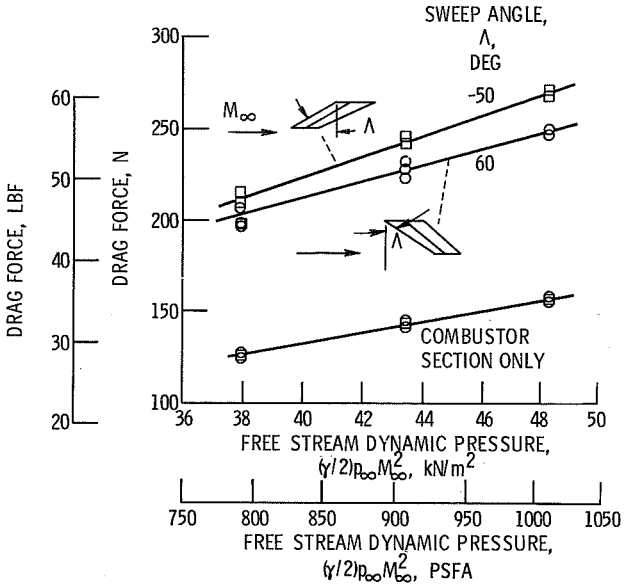

Figure 11. - Effect of sweep back and sweep forward on drag at Mach 2.5 with strut number 5.

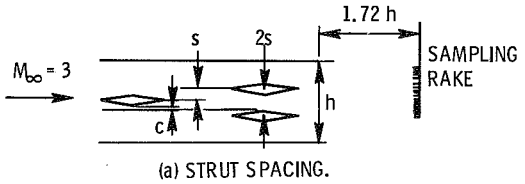

(a) STRUT SPACING.

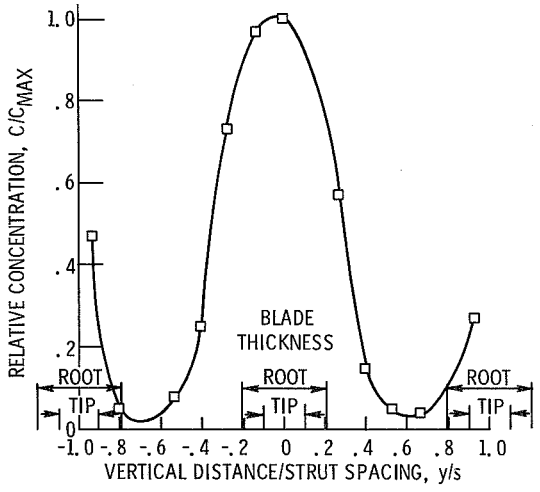

(b) HELIUM DISTRIBUTION MEASUREMENT.

Figure 12. - Strut spacing and helium distribution measurement with number 8 struts for Mach 3. Mass flow ratio of helium to air, 0.021; z/h, 0.222.

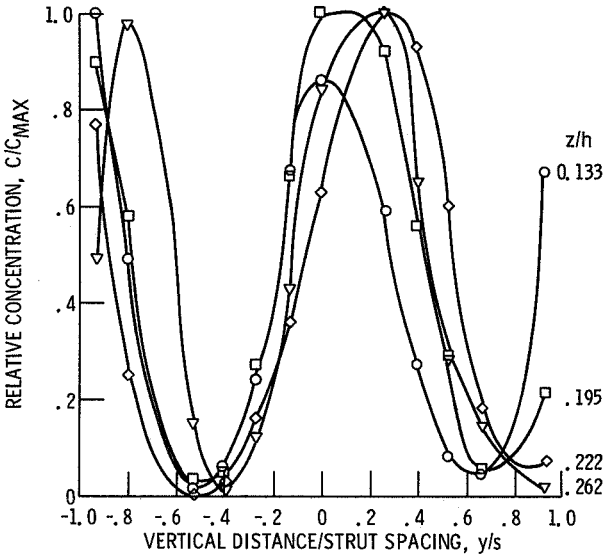

Figure 13. - Helium distribution at various lateral stream positions with number 5 struts at Mach 3. Mass flow ratio of helium to air, 0.032; x/h, 4.50.

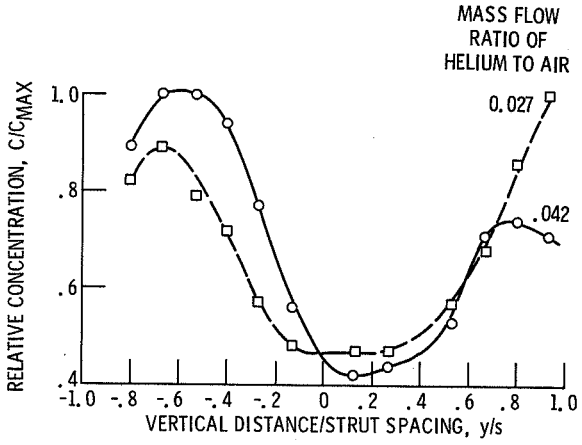

Figure 14. - Helium distribution for variable helium to air with number 2 struts at Mach 2.5. x/h, 4.50; z/h, 0.222.

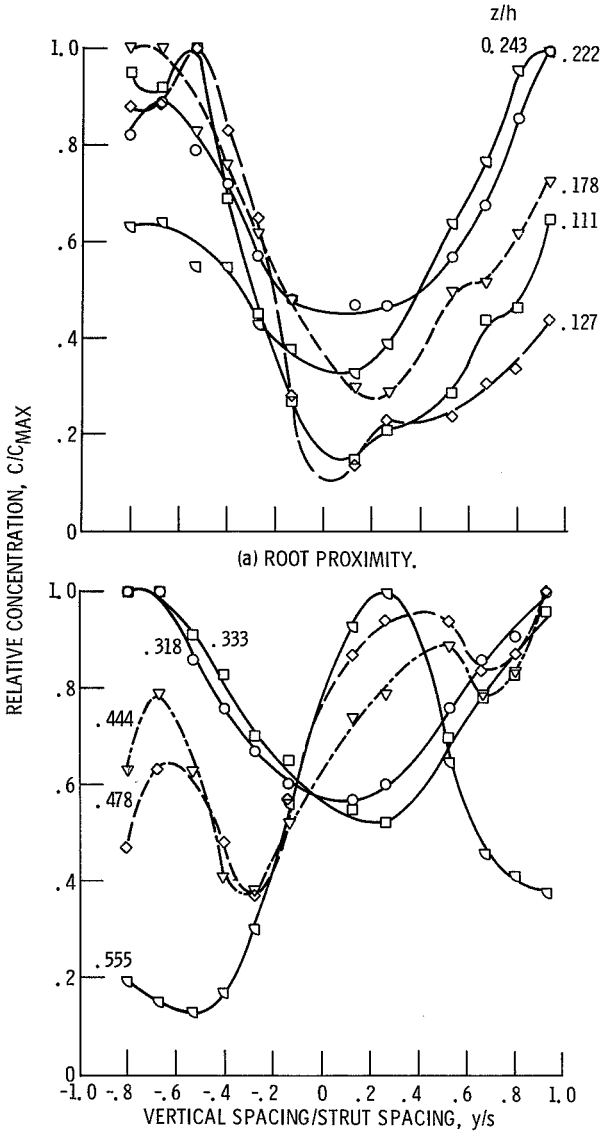

Figure 15. - Helium distribution at various lateral stream positions with number 2 struts at Mach 2.5. Mass flow ratio of helium to air, 0.027; x/h, 4.50.

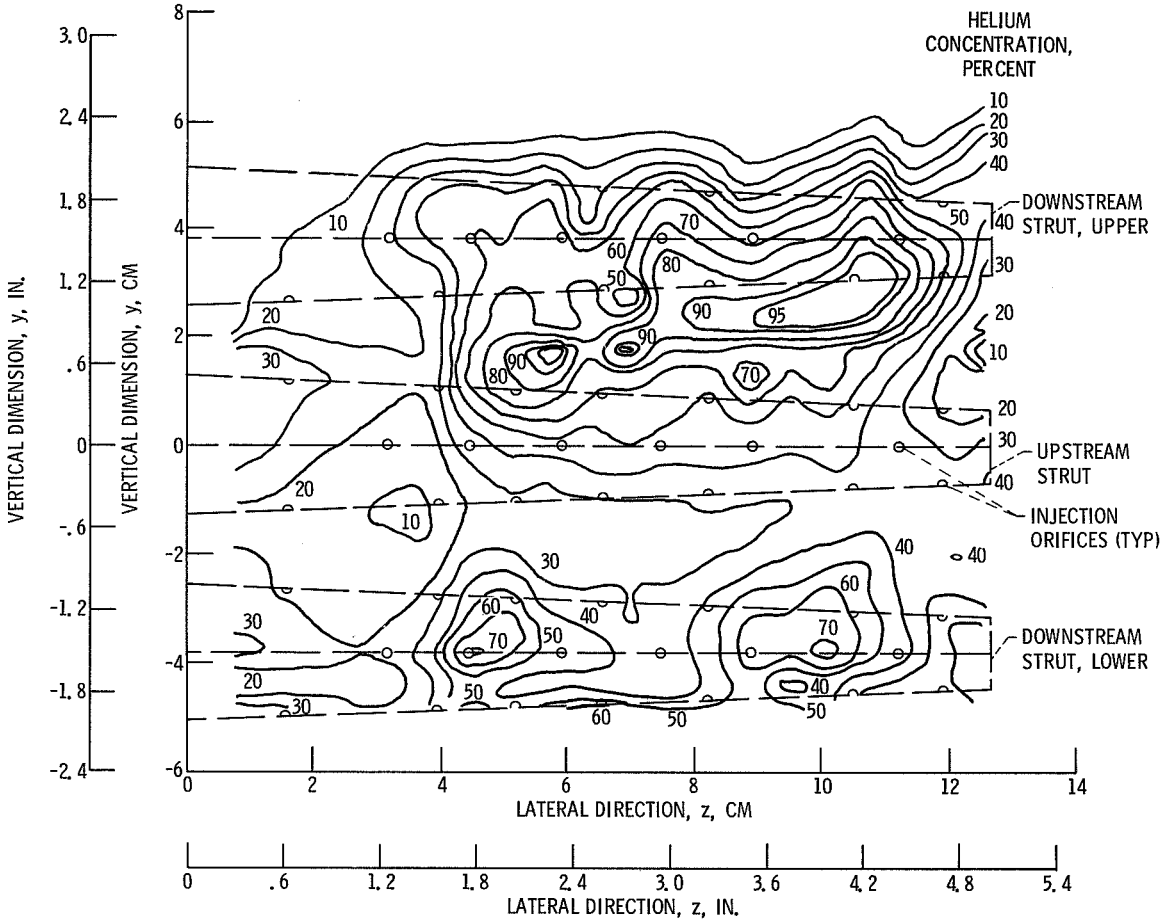

Figure 16. - Helium distribution controus with number 2 struts at Mach 2.5. Final modification; mass flow ratio of helium to air, 0.031; x/h, 4.50.

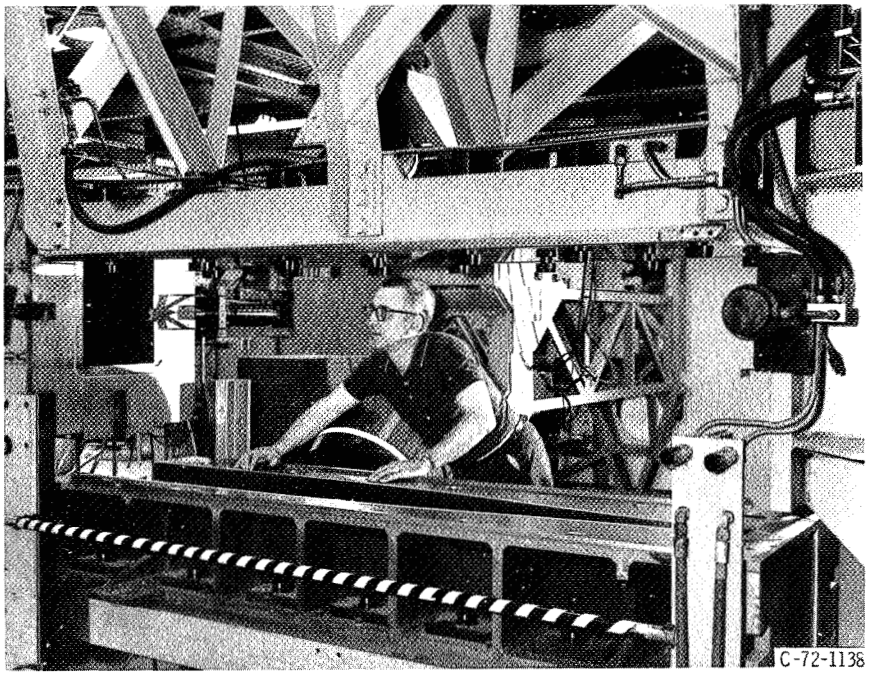

Figure 17. - Calibration rake installation.

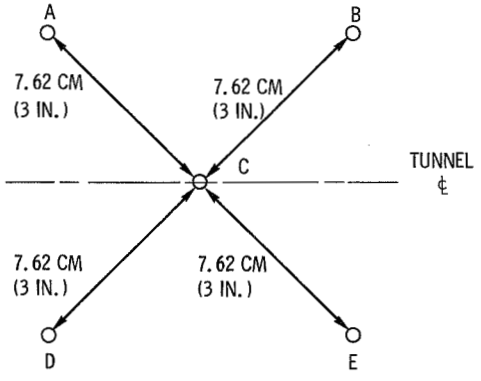

Figure 18. - Spacing arrangement on pitot tube calculation rake.

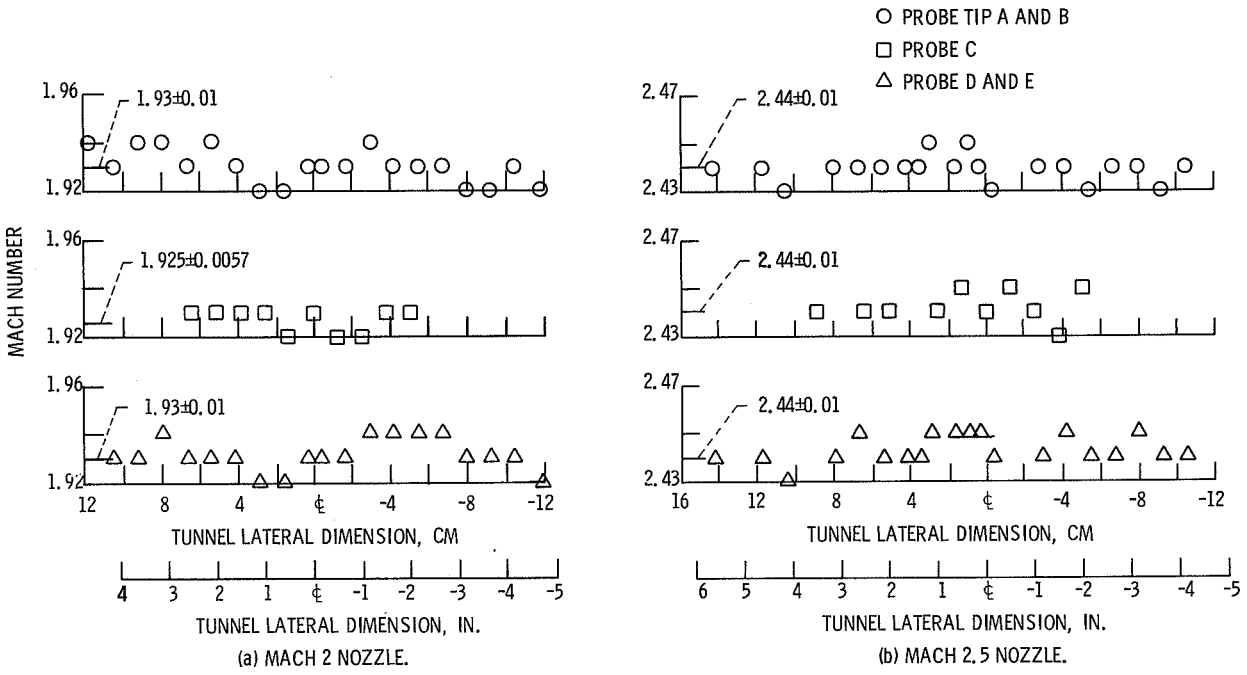

Figure 19. - Nozzle calibration.

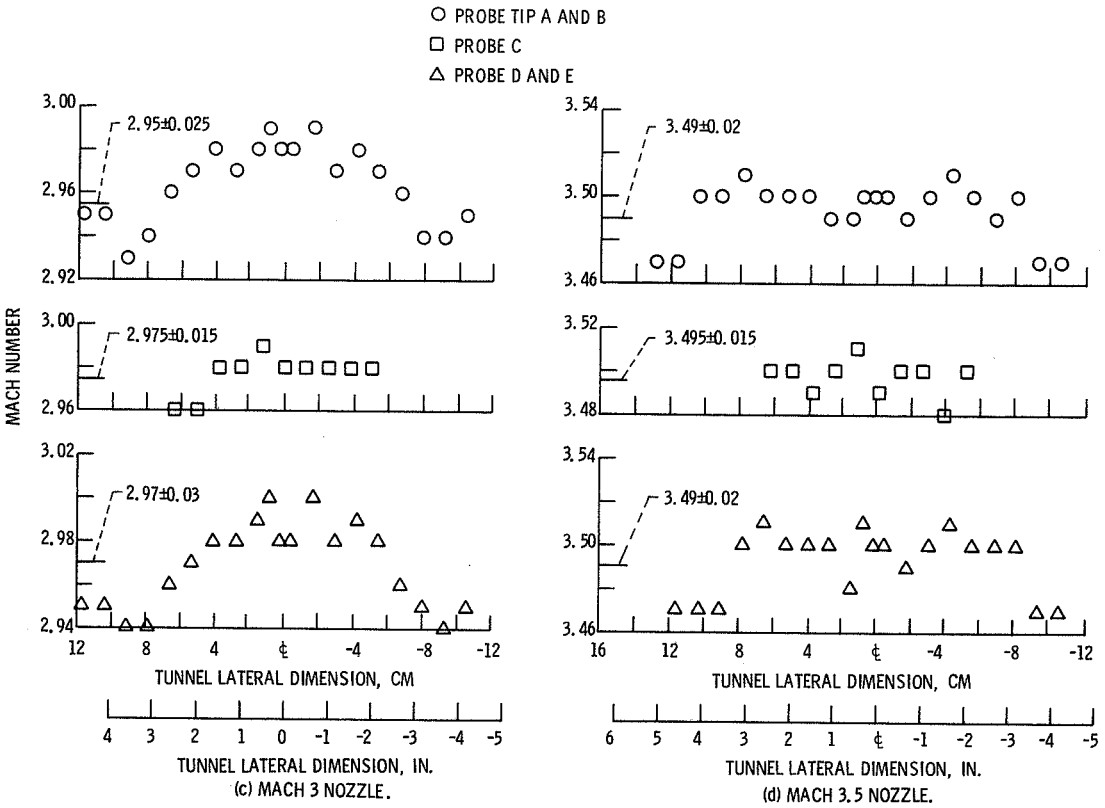

(c) MACH 3 NOZZLE.

(d) MACH 3.5 NOZZLE.

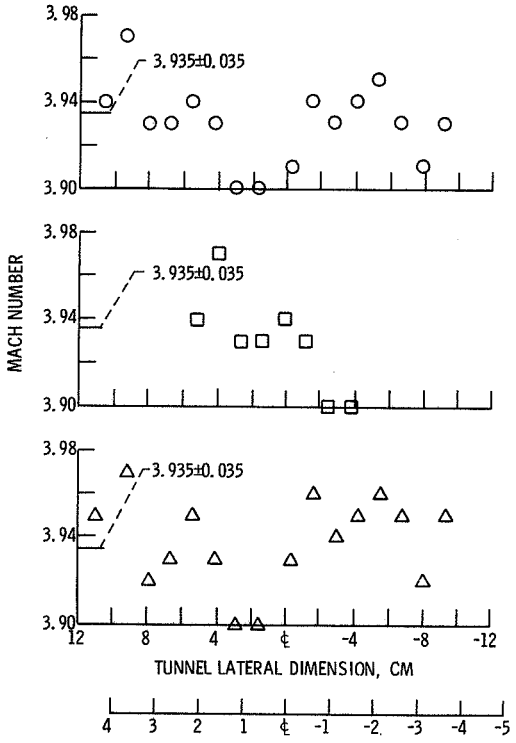

(e) MACH 4 NOZZLE.

Figure 19. - Concluded.

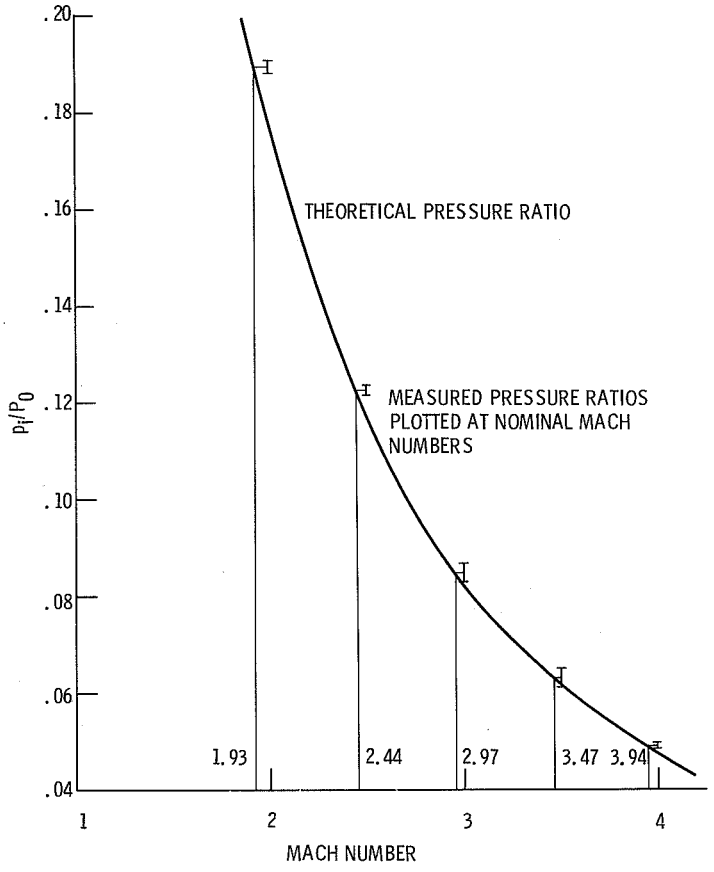

Figure 20. - Measured pressure ratio plotted against Mach number.

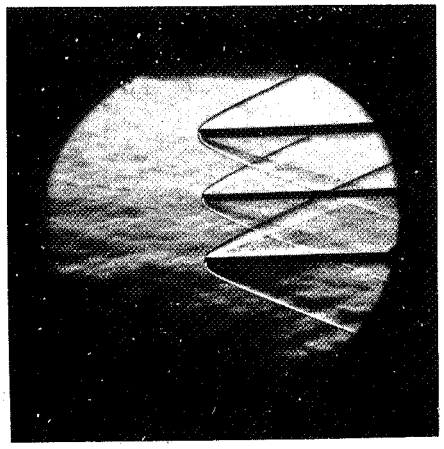

Figure 21. - Schlieren photograph of calibration rake at Mach 2.5 (nominal).

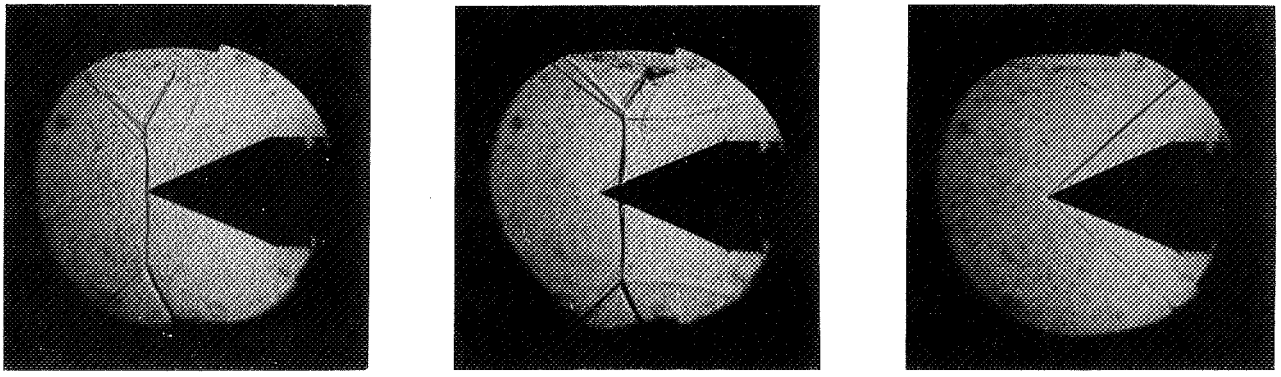

(a) Starting shock at cone apex. (b) Starting shock past cone apex. (c) Started condition.

Figure 22. - Tunnel starting sequence for 45° cone at Mach 2.0.

(a) Starting shock upstream of model. (b) Starting shock past cone apex. (c) Maximum progression of starting shock.

Figure 23. - Schlieren sequence of nonstarted condition at Mach 2.5.

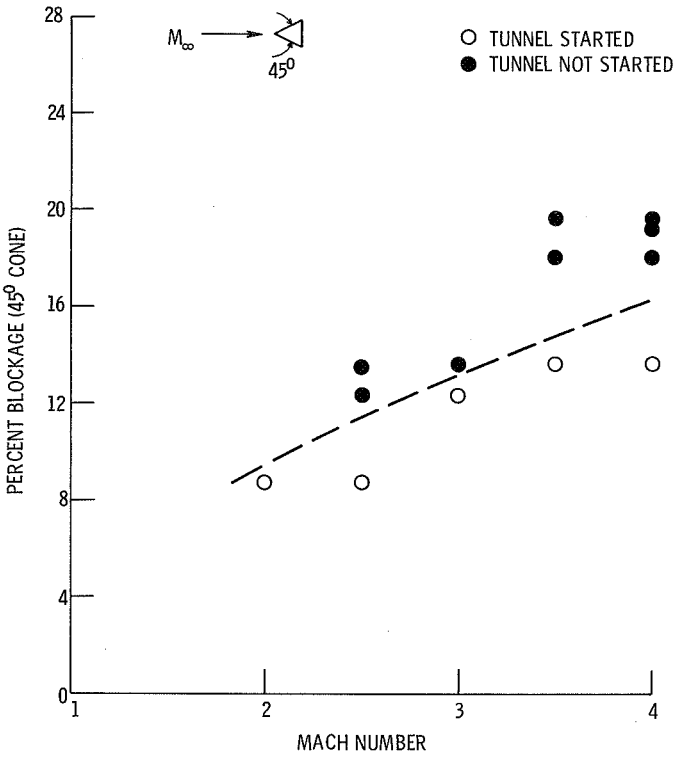

Figure 24. - Blockage test results, 0.31- by 0.31-meter (1- by 1-ft) block tunnel. P_{0_∞} = 276 kN/m^2 (40 psig).

NASA-Langley, 1974 E-7849

NATIONAL AERONAUTICS AND SPACE ADMINISTRATION
WASHINGTON, D.C. 20546

OFFICIAL BUSINESS
PENALTY FOR PRIVATE USE $300

SPECIAL FOURTH-CLASS RATE BOOK

POSTAGE AND FEES PAID
NATIONAL AERONAUTICS AND SPACE ADMINISTRATION
451

U.S.MAIL

POSTMASTER: If Undeliverable (Section 158 Postal Manual) Do Not Return

"The aeronautical and space activities of the United States shall be conducted so as to contribute . . . to the expansion of human knowledge of phenomena in the atmosphere and space. The Administration shall provide for the widest practicable and appropriate dissemination of information concerning its activities and the results thereof."

—NATIONAL AERONAUTICS AND SPACE ACT OF 1958

NASA SCIENTIFIC AND TECHNICAL PUBLICATIONS

TECHNICAL REPORTS: Scientific and technical information considered important, complete, and a lasting contribution to existing knowledge.

TECHNICAL NOTES: Information less broad in scope but nevertheless of importance as a contribution to existing knowledge.

TECHNICAL MEMORANDUMS: Information receiving limited distribution because of preliminary data, security classification, or other reasons. Also includes conference proceedings with either limited or unlimited distribution.

CONTRACTOR REPORTS: Scientific and technical information generated under a NASA contract or grant and considered an important contribution to existing knowledge.

TECHNICAL TRANSLATIONS: Information published in a foreign language considered to merit NASA distribution in English.

SPECIAL PUBLICATIONS: Information derived from or of value to NASA activities. Publications include final reports of major projects, monographs, data compilations, handbooks, sourcebooks, and special bibliographies.

TECHNOLOGY UTILIZATION PUBLICATIONS: Information on technology used by NASA that may be of particular interest in commercial and other non-aerospace applications. Publications include Tech Briefs, Technology Utilization Reports and Technology Surveys.

Details on the availability of these publications may be obtained from:

SCIENTIFIC AND TECHNICAL INFORMATION OFFICE

NATIONAL AERONAUTICS AND SPACE ADMINISTRATION

Washington, D.C. 20546